

Inactivation of Gating Currents of L-Type Calcium Channels

Specific Role of the $\alpha_2\delta$ Subunit

ROMAN SHIROKOV, GONZALO FERREIRA, JIANXUN YI, and EDUARDO RÍOS

From the Department of Molecular Biophysics and Physiology, Rush University School of Medicine, Chicago, Illinois 60612

ABSTRACT In studies of gating currents of rabbit cardiac Ca channels expressed as α_{1C}/β_{2a} or $\alpha_{1C}/\beta_{2a}/\alpha_2\delta$ subunit combinations in tsA201 cells, we found that long-lasting depolarization shifted the distribution of mobile charge to very negative potentials. The phenomenon has been termed charge interconversion in native skeletal muscle (Brum, G., and E. Ríos. 1987. *J. Physiol. (Camb.)*. 387:489–517) and cardiac Ca channels (Shirokov, R., R. Levis, N. Shirokova, and E. Ríos. 1992. *J. Gen. Physiol.* 99:863–895). Charge 1 (voltage of half-maximal transfer, $V_{1/2} \approx 0$ mV) gates noninactivated channels, while charge 2 ($V_{1/2} \approx -90$ mV) is generated in inactivated channels. In α_{1C}/β_{2a} cells, the available charge 1 decreased upon inactivating depolarization with a time constant $\tau \approx 8$, while the available charge 2 decreased upon recovery from inactivation (at -200 mV) with $\tau \approx 0.3$ s. These processes therefore are much slower than charge movement, which takes <50 ms. This separation between the time scale of measurable charge movement and that of changes in their availability, which was even wider in the presence of $\alpha_2\delta$, implies that charges 1 and 2 originate from separate channel modes. Because clear modal separation characterizes slow (C-type) inactivation of Na and K channels, this observation establishes the nature of voltage-dependent inactivation of L-type Ca channels as slow or C-type. The presence of the $\alpha_2\delta$ subunit did not change the $V_{1/2}$ of charge 2, but sped up the reduction of charge 1 upon inactivation at 40 mV (to $\tau \approx 2$ s), while slowing the reduction of charge 2 upon recovery ($\tau \approx 2$ s). The observations were well simulated with a model that describes activation as continuous electrodiffusion (Levitt, D. 1989. *Biophys. J.* 55:489–498) and inactivation as discrete modal change. The effects of $\alpha_2\delta$ are reproduced assuming that the subunit lowers the free energy of the inactivated mode.

KEY WORDS: cardiac muscle • heterologous expression • continuum model of gating • charge interconversion • charge immobilization

INTRODUCTION

Voltage-dependent inactivation of Ca channels is an important mechanism of regulation of Ca^{2+} entry during repetitive stimulation. Its relatively slow kinetics allow for a long-term, direct control of channel availability by transmembrane electric potential. Although inactivation is thought to be a property of the α_1 subunit, fine tuning of its voltage sensitivity depends on interactions with auxiliary subunits and with other proteins.

In spite of a resemblance between voltage-dependent inactivation of Ca channels and the so-called slow or C-type inactivation found in the whole superfamily of voltage-gated channels, the structural underpinnings of this process have yet to be identified in Ca channels. Slow inactivation may be characterized by its relatively slow kinetics ($\tau \approx 1$ s), dependence on extracellular cations,

and involvement of the extracellular portions of pore forming S5-S6 linkers (Brum et al., 1988; Hoshi et al., 1990; López-Barneo et al., 1993; Yellen et al., 1994; Balser et al., 1996; Townsend and Horn, 1997). In addition, slow inactivation is believed to result in the appearance of a specific intramembranous charge movement (charge 2; Brum and Ríos, 1987) generated by conformational changes in inactivated channels (Bezanilla et al., 1982; Brum and Ríos, 1987; Shirokov et al., 1992; Olcese et al., 1997). Slow rates of inactivation and recovery are essential for the operational separation of two types of charge. Charge 2 is well defined and separate from charge 1 (the charge that moves in noninactivated or primed channels) because its observable movement proceeds to completion much sooner than inactivation onset or recovery.

In contrast, fast inactivation of Na channels and N-type inactivation of *Shaker* K channels (ball and chain type; Armstrong and Bezanilla, 1977; Vassilev et al., 1988; Zagotta et al., 1990) recovers rapidly at negative potentials, approximately simultaneously with the inward movement of the intramembranous charge. Because recovery may proceed at rates comparable with that of measurable charge movement, there is no well-defined mode of charge movement that can be ascribed to this

Dr. Ferreira's permanent address is Depto. Biofísica, Facultad de Medicina, Montevideo, Uruguay CP 11800. Dr. Shirokov's permanent address is A.A. Bogomoletz Institute of Physiology, Kiev, Ukraine 252024.

Address correspondence to Roman Shirokov, Department of Molecular Biophysics and Physiology, Rush University School of Medicine, 1750 W. Harrison Street, Suite 1279JS, Chicago, IL 60612. Fax: 312-942-8711; E-mail: rshiroko@rush.edu

type of inactivation. The inward charge movement observed at large negative potentials after an inactivating depolarization occurs in channels as they recover from inactivation (repriming).

Apparently, a ball and chain-type inactivation is not present in Ca channels. It has been shown for several types of Ca channels that the faster component of ionic current decay is driven by ionic current itself. Because neither changes in intracellular calcium (Hadley and Lederer, 1992) nor the ion flow through cardiac channels influence inactivation of gating currents, Shirokov et al. (1993) concluded that Ca^{2+} -dependent inactivation is a separate process, linked to gating currents only indirectly, through channel opening.

We have shown previously that decay of Ba^{2+} current through L-type Ca channels constituted by α_{1C} and β_{2a} subunits occurs in two phases. The slow phase ($\tau \approx 8$ s) is associated with voltage-dependent inactivation and is cotemporal with the reduction of available gating charge upon inactivation at positive voltages (Ferreira et al., 1997). We now address in quantitative detail the inactivation of intramembranous charge movement in heterologously expressed α_{1C} channels. Because cardiac Ca channels transiently express at high density in the tsA201 human embryonic kidney cell line, we were able to measure intramembrane charge movements in these channels without using pulse protocols for subtraction of control records. This allowed us to study in detail the effects of conditioning voltage on the movement of voltage sensors, with or without the $\alpha_2\delta$ subunit, and develop a compact biophysical model that describes voltage-dependent inactivation well. The rate of the slow phase of Ba^{2+} current decay is three- to fivefold greater in the presence of the $\alpha_2\delta$ subunit (Ferreira et al., 1997) and is equal to that in native channels. The biophysical model described here reproduces in a parsimonious manner the effects of the $\alpha_2\delta$ subunit.

METHODS

Experiments were performed in tsA201 cells grown in DME medium (Sigma Chemical Co., St. Louis, MO) supplemented with 10% FBS (BioWhittaker, Walkersville, MD), 100 U/ml penicillin, and 0.1 mg/ml streptomycin (Sigma Chemical Co.) in 5% CO_2 . Rabbit α_{1C} , $\alpha_2\delta_a$, and rat β_{2a} cDNAs were subcloned in pCR3, pMT2, and pCMV plasmid vectors, respectively. High purity ($A_{260}/A_{280} \approx 1.90$) large-scale plasmid preparations were obtained using standard protocols (QIAGEN Inc., Chatsworth, CA). Transfections were carried out with 30 μg of each expression plasmid in two combinations ($\alpha_{1C} + \beta_{2a}$ and $\alpha_{1C} + \beta_{2a} + \alpha_2\delta_a$) on 100-mm Petri dishes using a calcium phosphate precipitation method (Chien et al., 1995). Electrophysiological recordings were made within 24–48 h after transfection on round nonclustered cells. No sizable ionic or gating currents were observed in tsA201 cells in the absence of transfection. After transfection, the fraction of cells selected and patched that had Ca^{2+} currents was $\sim 70\%$.

Records were obtained by a standard whole-cell patch clamp procedure using an Axopatch 200A amplifier (Axon Instruments,

Inc., Foster City, CA) and a 16-bit A/D-D/A converter card (HSDAS 16; Analogic Corp., Peabody, MA) on a PC computer. Patch electrodes were pulled from Corning 7052 glass (Warner Instruments, Hamden, CT) and had resistances of 1.0–1.5 $\text{M}\Omega$.

The pipette solution contained (mM): 150 CsOH, 110 glutamate, 20 HCl, 10 HEPES, 5 MgATP, and 10 EGTA, pH 7.6. External recording solutions contained 160 TEA-Cl, 10 Tris, and 10 CaCl_2 , pH 7.2. To record intramembranous charge movement, the bath solution was replaced with one that included 15 μM of GdCl_3 . All solutions were adjusted to 300–320 mosmol/Kg. All experiments were carried out at room temperature ($\sim 20^\circ\text{C}$).

Whole-cell capacitance was 6–15 pF. The time constant of membrane charging typically did not exceed 100 μs . Series resistance, calculated from the capacitive transient, was below 10 $\text{M}\Omega$. The single time constant capacitance compensation circuitry of the Axopatch 200A amplifier was routinely used to offset 95–98% of the symmetric capacitive transient. Parameters of the compensation circuitry were set with a 10-mV pulse from the holding potential of -90 mV.

For a 200-mV pulse spanning most of the useful voltage range, the residual linear transient corresponded to a transfer of <10 fC/pF of charge, while maximal intramembranous charge transfer from the expressed channels was ~ 100 fC/pF. With this combination of a relatively fast voltage clamp, high level of expression, and effective linear capacitance compensation, we were able to record asymmetric capacitive transients directly, without acquiring control linear transients for further subtraction.

Gating currents were recorded at 1 kHz bandwidth and sampled at 10 kHz. During prolonged pulses, the sampling rate was switched to between 0.05 and 2 kHz. To let the channels recover from inactivation, sets of conditioning and test pulses were separated by 30 s or longer. Charge transfer was calculated as the time integral of the current transient after subtraction of a steady current, which was determined as a 10-ms average, 40 ms after the beginning of the pulse.

Fig. 1 illustrates a typical experiment. The pulse protocol is shown at top. A conditioning pulse of 20 s at 40 mV was applied before each test pulse. Conditioning and test pulses were separated by an interval at -20 mV. Current traces were obtained with different test pulse voltages (V). The charge transferred by the ON transients (\bullet) and the steady current during the test pulse (\square) are plotted against voltage in Fig. 1 B. The steady current–voltage relationship was linear in the range from -150 to 50 mV, with steepness corresponding to an input resistance of ~ 5 $\text{G}\Omega$. The steady current at 0 mV was ~ -3 pA. The charge transfer–voltage relationship was clearly sigmoidal, saturating at extreme voltages. This demonstrates that the contribution of the linear capacitance was small, and validates the evaluation of charge transfer without subtraction of control currents.

Data are presented as averages \pm SEM. Significance of differences between mean values was evaluated by Student's *t* test. Voltage distributions and time courses were fitted, respectively, by single Boltzmann and single exponential functions using a nonlinear least-squares routine included in the Sigmaplot software package (SPSS Inc., Chicago, IL).

RESULTS

Steady State Distributions of Charge Movement in Primed and Inactivated Channels

To study effects of conditioning depolarization on the voltage dependence of intramembranous charge movement, we used a double pulse protocol illustrated in Fig. 2. First, gating currents were recorded in polarized

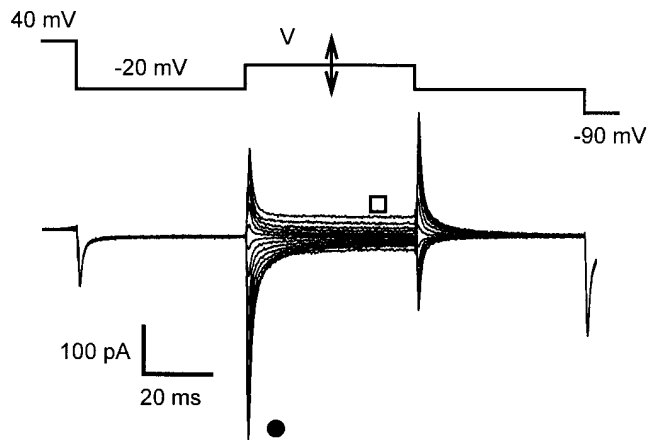
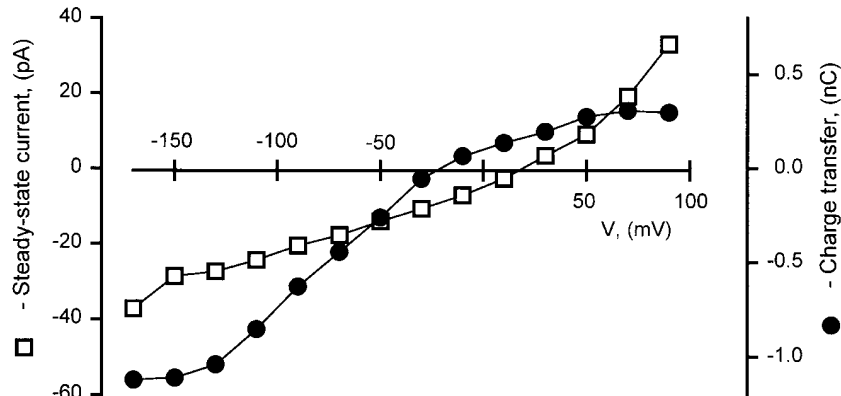
A**B**

FIGURE 1. Evaluating quality of analog subtraction of the linear capacitance. (A) Intramembrane charge movement records obtained with analog subtraction of symmetric capacitive transient as described in METHODS. Pulse protocol is shown at top. Currents were elicited in an α_1/β cell by pulses to test voltages (V) between -190 and 90 mV in increments of 20 mV. Every test pulse was preceded by a 20 -s long conditioning to 40 mV. Symbols correspond to plots in B. (B) Charge transferred during the ON transient (\bullet) and steady current (\square) in traces shown in A, plotted against V.

α_1/β cells held at -90 mV (Fig. 2 A). The test pulse was applied from a 50 -ms long interpulse at -60 mV. Then the same protocol was applied again but with a 20 -s long conditioning pulse to 40 mV preceding each interpulse (Fig. 2 B). Current traces are shown on both panels for a set of test voltages starting at -190 mV in 40 -mV increments. There was little charge movement current at voltages more negative than -70 mV in polarized cells, but the conditioning produced a substantial increase of currents at these negative voltages. The charge transferred during the ON transient for the same cell is plotted against membrane potential in Fig. 2 C. When the cell was held at -90 mV, and consequently the channels were available for opening, most of the charge moved during pulses positive to -60 mV (Fig. 2, \bullet). In inactivated channels, by contrast, about half of the charge moved in pulses below -60 mV (Fig. 2, \circ). Curves are fits by a shifted Boltzmann function

$$Q(V) = Q_0 + Q_{\text{MAX}} / (1 + \exp[(V - V_{1/2})/K]), \quad (1)$$

where Q_0 , a negative quantity, is the limit of charge transfer as V tends to $-\infty$, Q_{MAX} is the difference between the maximal positive transfer and Q_0 , $V_{1/2}$ is the voltage of half-maximal transfer, or transition potential, and K is a steepness constant. The measurable charge movement during the interpulse had ended by the end of the interpulse. Therefore, the changes in charge distribution in inactivated channels were long-lived compared with the time scale of the measurable charge movement.

Addition of the $\alpha_2\delta$ subunit increased the effect of depolarization on charge transfer. About two thirds of the charge was mobile below -60 mV in inactivated $\alpha_1/\beta/\alpha_2\delta$ channels (Fig. 3). To compare the effects of conditioning in α_1/β and $\alpha_1/\beta/\alpha_2\delta$ cells, we averaged charge distributions obtained in different cells, normalized as follows. First, Eq. 1 was fitted to individual $Q(V)$ data, and the fitted shift Q_0 was subtracted from $Q(V)$. Data shifted in this way (referred to as "charge distributions") can be compared without reference to starting

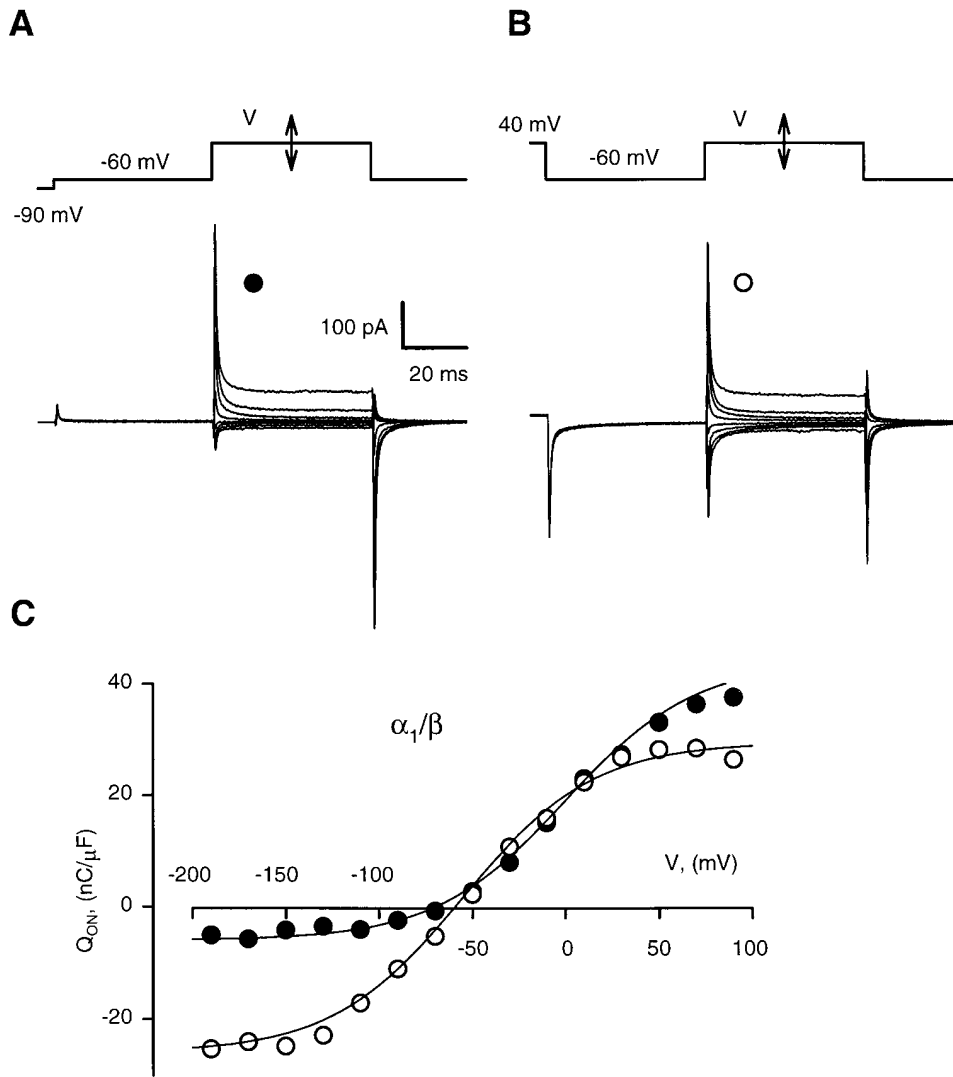


FIGURE 2. Conditioning depolarization shifts to negative voltages charge transfer in α_1/β cells. (A) Gating current transients in a nonconditioned α_1/β cell. Shown are the currents elicited with test pulses to voltages ranging from -190 to 90 mV, in 40 -mV intervals, starting from a 50 -ms long interpulse at -60 mV. (B) Gating currents in the same cell, conditioned by a 20 -s long pulse to 40 mV applied before each test pulse. (C) Charge transfer without (●) and with (○) conditioning, calculated from the records illustrated in A and B and plotted vs. V . Smooth lines are drawn by: $Q(V)$ (nC/ μ F) = $-6 + 50/[1 + \exp(V/35 \text{ mV})]$ for primed, and $Q(V)$ (nC/ μ F) = $-26 + 55.5/(1 + \exp[(V + 55 \text{ mV})/35 \text{ mV}])$ for the inactivated cell.

voltage. For averaging, the charge distribution was normalized to the individual Q_{MAX} determined in the inactivated cell.¹ Averages of normalized distributions are shown in Fig. 4. The curves are Boltzmann fits with parameters listed in Table I. In polarized cells (Fig. 4, ●), $V_{1/2}$ was close to 0 mV, but some 12 mV more negative in α_1/β (-8.4 mV) than in $\alpha_1/\beta/\alpha_2\delta$ cells (3.9 mV). One reason for this small difference is that gating charge in the primed cells is systematically underestimated at voltages positive to 70 mV (and $V_{1/2}$ is conse-

quently undervalued), due to the presence of nonspecific outward current. With the $\alpha_2\delta$ subunit present, maximal charge movement increases approximately twofold (Bangalore et al., 1996), which makes the relative error smaller and $V_{1/2}$ greater.

When charge transfers were measured after the inactivating pulse (Fig. 4, ○), $V_{1/2}$ was shifted by -57 mV in α_1/β cells and by -81 mV in $\alpha_1/\beta/\alpha_2\delta$ cells. The difference in shifts was statistically significant ($P < 0.05$). As shown in Table I, inactivation induced only minor changes in steepness and total mobile charge. As was the case for the distribution of charge movement in native cardiomyocytes (Shirokov et al., 1993), the effect of inactivation is best described, with either subunit composition, as a simple shift in the transition potential.

The greater shift in the presence of the $\alpha_2\delta$ subunit could be the result of a greater extent of inactivation during the conditioning pulse to 40 mV, a slower recov-

¹For example, charge transfer (nC/pF, V in mV) in the cell illustrated in Fig. 3 is fitted by $Q(V) = -2.5 + 59.6/[1 + \exp[(V - 6.8)/25.0]]$ in the nonconditioned case, and $Q(V) = -38.9 + 55.0/[1 + \exp[(V + 85.0)/31.8]]$ after conditioning. The normalized distributions in the same cell are, respectively: $Q'(V) = 1.08/[1 + \exp[(V - 6.8)/25.0]]$, and $Q'(V) = 1.00/[1 + \exp[(V + 85.0)/31.8]]$.

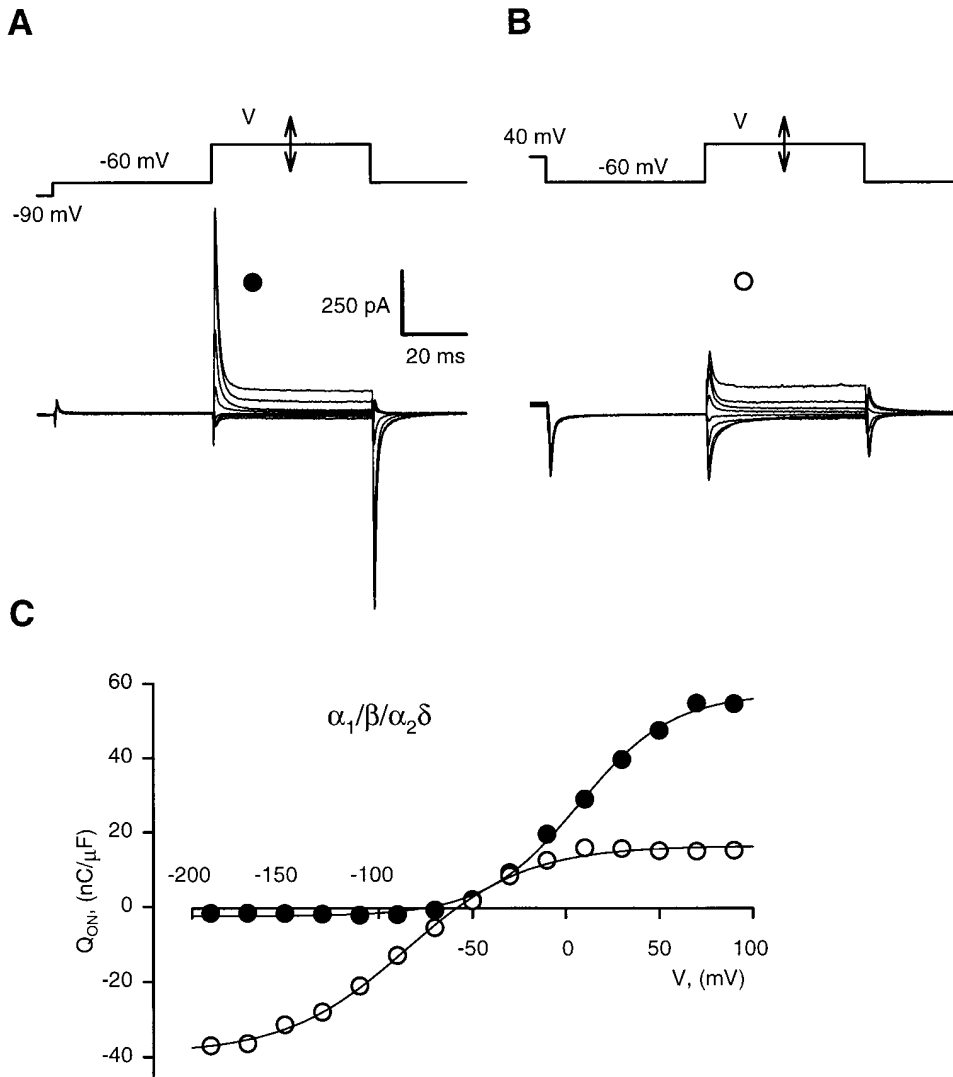


FIGURE 3. Greater negative shift of charge transfer in $\alpha_1/\beta/\alpha_2\delta$ cells. (A) Gating current transients in a nonconditioned $\alpha_1/\beta/\alpha_2\delta$ cell. As in Fig. 2, the records shown are of currents elicited with test pulses to voltages ranging from -190 to 90 mV, in 40 -mV intervals, starting from a 50 -ms long interpulse at -60 mV. (B) Gating currents in the same cell, conditioned by a 20 -s long pulse to 40 mV applied before each test pulse. (C) Charge transfer without (\bullet) and with (\circ) conditioning, calculated from the records in A and B and plotted vs. V. Smooth lines are drawn by: $Q(V)$ (nC/ μ F) = $-2.5 + 60 / (1 + \exp[(V - 7 \text{ mV})/25 \text{ mV}])$ for primed, and $Q(V)$ (nC/ μ F) = $-39 + 55 / (1 + \exp[(V + 85 \text{ mV})/32 \text{ mV}])$ for the inactivated cell.

ery from inactivation during the interpulse at -60 mV, or both. To test these possibilities, we studied voltage distributions of mobile charge after an inactivating pulse, varying the interpulse voltage.

In the extreme case illustrated in Fig. 5, there was no

interpulse. When negative-going test pulses were applied after a 50 -ms long step to 40 mV, as shown in Fig. 5 A for an $\alpha_1/\beta/\alpha_2\delta$ cell, charge transfer was nearly maximal at -100 mV (Fig. 5 C, \blacksquare). After a 20 -s long conditioning pulse, charge transfer at -100 mV was

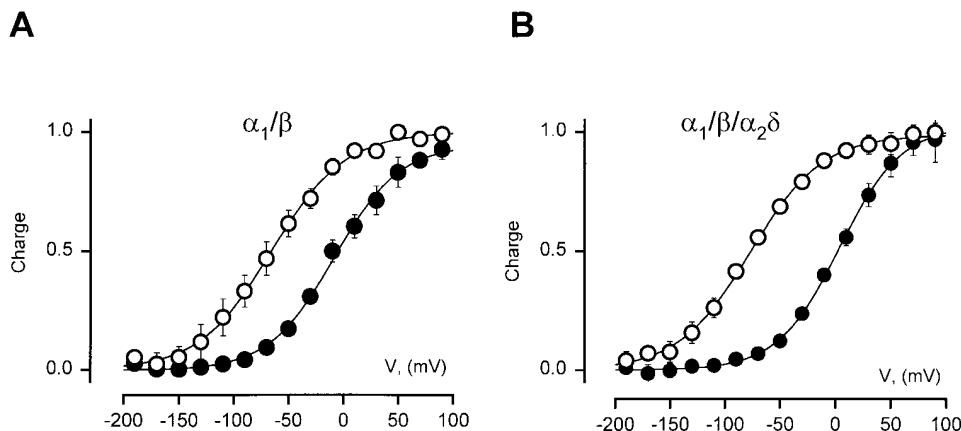


FIGURE 4. Effect of conditioning on charge distributions obtained with pulses from -60 mV. (A) Average charge distributions derived from charge transfer functions illustrated in Fig. 2, in nonconditioned (\bullet) and conditioned (\circ) α_1/β cells ($n = 8$). Smooth lines are fits with Boltzmann equation: $Q(V) = Q_{MAX} / (1 + \exp[(V - V_{1/2})/K])$. Best fit parameters are in Table I. (B) Average charge distributions in $\alpha_1/\beta/\alpha_2\delta$ cells ($n = 9$), derived from charge transfer functions illustrated in Fig. 3.

TABLE I

Composition	Interpulse voltage (mV)	n	$V_{1/2}$ (mV)		K (mV)		Q_{MAX}	
			Reference	Conditioned	Reference	Conditioned	Reference	Conditioned
α_1/β	-60	14	-8.4 ± 2.0	-65.5 ± 1.7	29.6 ± 1.5	33.4 ± 1.4	0.95 ± 0.02	1.00 ± 0.01
	+40	5	-20.3 ± 3.3	-89.6 ± 2.9	39.2 ± 3.4	39.6 ± 2.4	0.93 ± 0.05	1.02 ± 0.04
	-150	5	1.5 ± 4.8	-17.5 ± 1.7	31.6 ± 3.7	31.1 ± 1.6	1.03 ± 0.06	1.00 ± 0.02
$\alpha_1/\beta/\alpha_2\delta$	-60	9	3.9 ± 1.2	-77.3 ± 1.1	27.9 ± 0.8	32.8 ± 0.9	1.02 ± 0.01	0.99 ± 0.01
	+40	5	-21.8 ± 2.4	-90.4 ± 2.3	38.9 ± 2.6	30.6 ± 1.9	0.96 ± 0.04	1.01 ± 0.04
	-150	5	2.9 ± 1.5	-33.9 ± 1.1	27.6 ± 1.3	28.0 ± 1.0	0.93 ± 0.02	0.98 ± 0.02

Parameters of single Boltzmann function $Q(V) = Q_{MAX}/(1 + \exp(V - V_{1/2})/K)$ fitted to voltage dependencies of intramembrane charge movement in tsA201 cells transfected with α_1/β and $\alpha_1/\beta/\alpha_2\delta$ combinations of L-type Ca^{2+} channel subunits. The distributions were determined from different interpulse voltages as illustrated by pulse protocols on Figs. 2, 3, 5, and 6. The corresponding functions are plotted on Figs. 4-6.

only about half-maximal (Fig. 5 C, \square). Fig. 5 D plots the corresponding distributions in $\alpha_1/\beta/\alpha_2\delta$ cells. For comparison, the dashed curves are the best fits in α_1/β cells. Addition of the $\alpha_2\delta$ subunit did not change significantly the transition potentials in noninactivated or inactivated channels. The only significant difference was that charge distribution of inactivated channels was somewhat steeper in the presence of the $\alpha_2\delta$ subunit.

The experiments in Fig. 5 indicate that the difference in distributions after conditioning demonstrated in Fig. 4 was mostly due to a faster recovery of α_1/β cells during the interpulse at -60 mV. In the absence of an interpulse allowing recovery, the difference induced by inactivation was about the same with both subunit compositions.

When test pulses were applied from an interpulse

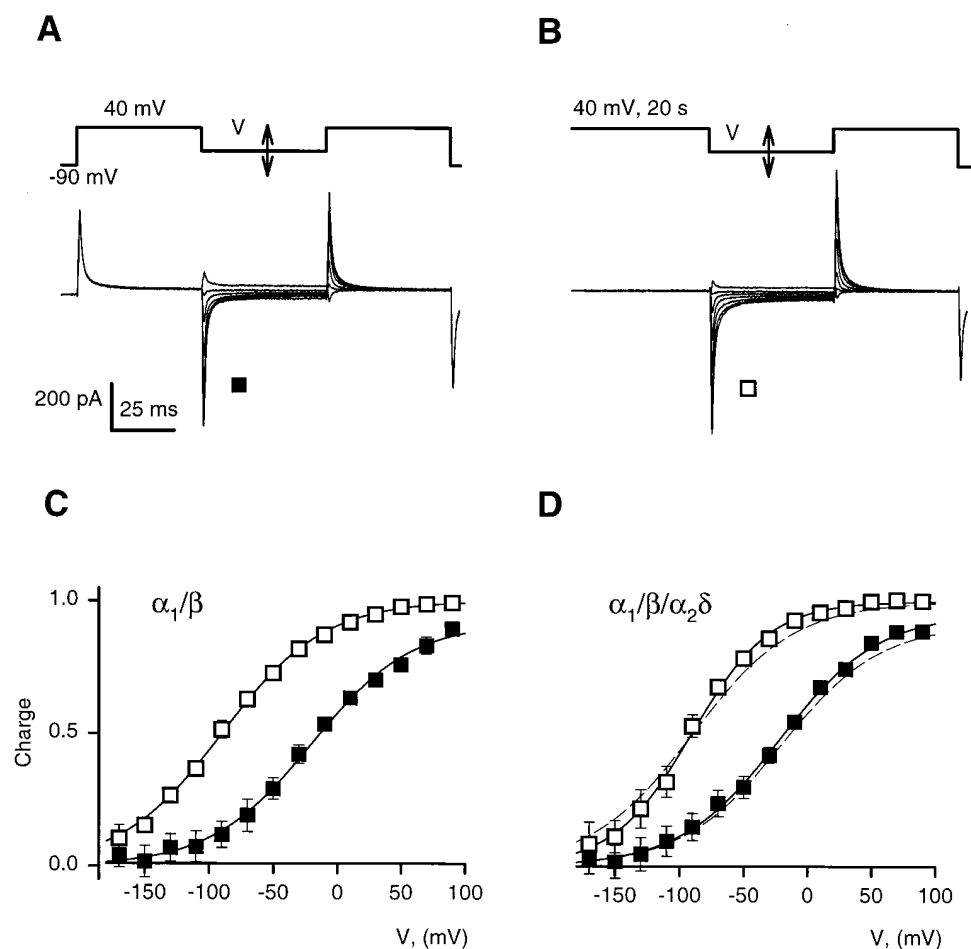


FIGURE 5. Effect of conditioning on charge distributions obtained with pulses from 40 mV. (A) Gating currents elicited in an $\alpha_1/\beta/\alpha_2\delta$ cell. Shown are the currents elicited with test pulses to voltages ranging from -170 to 90 mV in 40-mV intervals, starting from a 50-ms long interpulse at 40 mV. (B) Gating currents in the same cell, elicited by test pulses from a 20-s long conditioning at 40 mV. (C) Average charge distributions in α_1/β cells ($n = 5$), calculated from charge transfers obtained as illustrated in A and B. (■) Charge distribution after a 50-ms long prepulse to 40 mV. (□) Charge distribution after a 20-s long conditioning. Solid lines are Boltzmann fits through the data. (D) Corresponding average charge distributions in $\alpha_1/\beta/\alpha_2\delta$ cells ($n = 5$). Solid lines are Boltzmann fits through the data. Dashed lines copy the fits (shown in C) to average charge distributions without the $\alpha_2\delta$ subunit. The transition potentials of the distributions obtained after 20-s long conditioning are not significantly different in $\alpha_1/\beta/\alpha_2\delta$ and α_1/β cells (Table I).

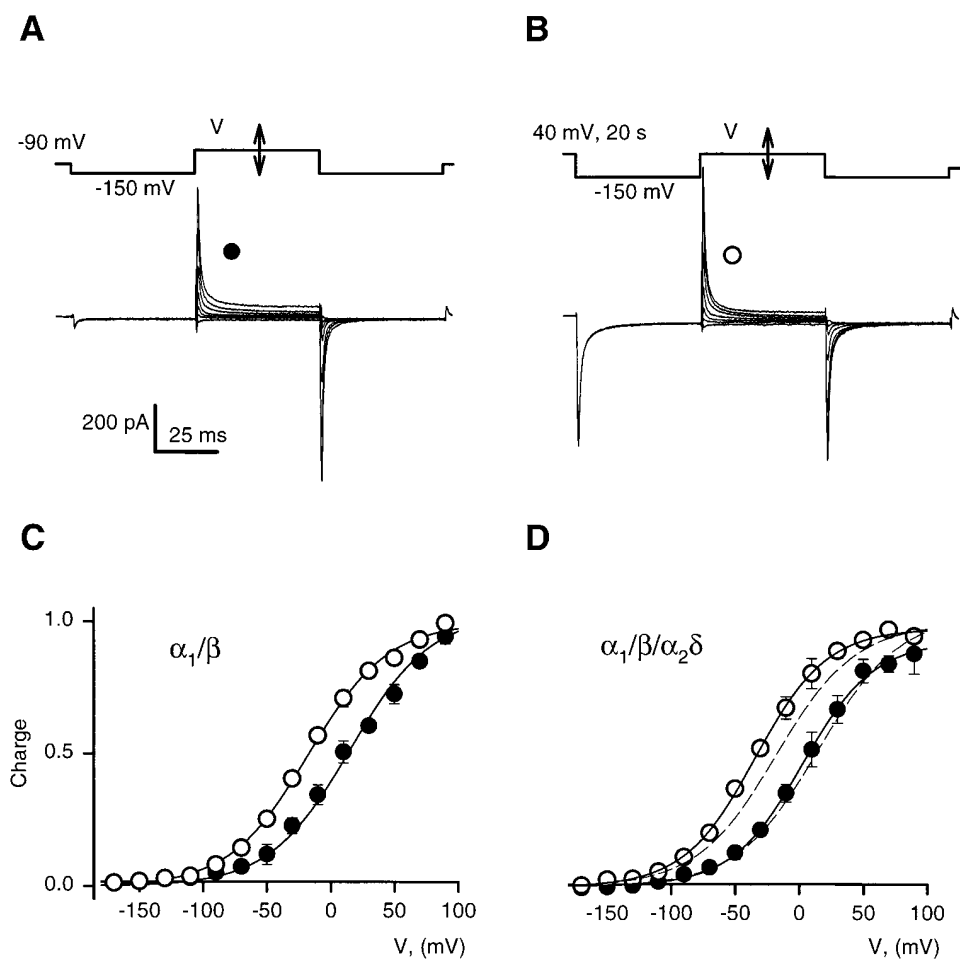


FIGURE 6. Effect of conditioning on charge distributions obtained with pulses from -150 mV. (A) Gating currents elicited in an $\alpha_1/\beta/\alpha_2\delta$ cell. Shown are the currents elicited with test pulses to voltages ranging from -170 to 90 mV, in 40 -mV intervals, starting from a 50 -ms long interpulse at -150 mV. (B) Gating currents in the same cell, when the interpulses are preceded by a 20 -s long conditioning at 40 mV. (C) Average charge distributions in α_1/β cells. (D) Average charge distributions in $\alpha_1/\beta/\alpha_2\delta$ cells, with the fits to the distributions in α_1/β cells represented in dashed trace. The data set is from the same cells as in Fig. 5. Note that the charge distribution in conditioned $\alpha_1/\beta/\alpha_2\delta$ cells is considerably more shifted than in α_1/β cells (and the fitted transition potentials, listed in Table I, are significantly different).

level of -150 mV, conditioning again led to a negative shift of the charge distribution, now manifested as an increase of gating currents recorded at intermediate voltages, as shown for an $\alpha_1/\beta/\alpha_2\delta$ cell in Fig. 6, A and B. As shown in Fig. 6 D, the charge distribution in primed cells was affected little by the presence of the $\alpha_2\delta$ subunit (Fig. 6, ●). In conditioned $\alpha_1/\beta/\alpha_2\delta$ cells, however, the charge distribution was shifted to more negative voltages than in α_1/β cells, as a consequence of a slower recovery at -150 mV in the presence of the $\alpha_2\delta$ subunit. Again, the charge movement currents ended earlier than the interpulse, indicating that even at -150 mV the voltage shift in distribution of mobile charge induced by inactivation recovers much more slowly than the measurable return of the mobile charge.

These experiments demonstrate that in inactivated Ca channels all the charge remains mobile, albeit at voltages more negative than those of activation gating. The concept of modal conversion applicable to slow inactivation of native Na channels (Bezanilla et al., 1982), recombinant *Shaker* K channels (Olcese et al., 1997), and voltage-dependent inactivation of native Ca channels of skeletal (Brum and Ríos, 1987) and cardiac

muscle (Shirokov et al., 1992) is seen to apply to recombinant Ca channels. Gating transitions within the primed mode of the channel produce charge 1 movements, while transitions within the inactivated mode produce sterile charge 2.

The present results suggest that the $\alpha_2\delta$ subunit has little direct effect on charge 1 and charge 2 movements. Apparently, its main effects are on the kinetics of charge 1–charge 2 interconversion. We confirmed this impression with the experiments described below.

Kinetics of Inactivation of Charge Movement and Effects of the $\alpha_2\delta$ Subunit

Time-dependent inactivation of Ba^{2+} current through L-type Ca channels has two kinetic phases. In the absence of the $\alpha_2\delta$ subunit, prolonged depolarization reduces gating charge mobile above -60 mV with a time course parallel to the slower exponential component of Ba^{2+} current decay (Ferreira et al., 1997). The time constant of this component in α_1/β cells is ~ 8 s at 20 mV, while in $\alpha_1/\beta/\alpha_2\delta$ and in native cells it is ~ 2 s. In the experiment illustrated in Fig. 7, we investigated the

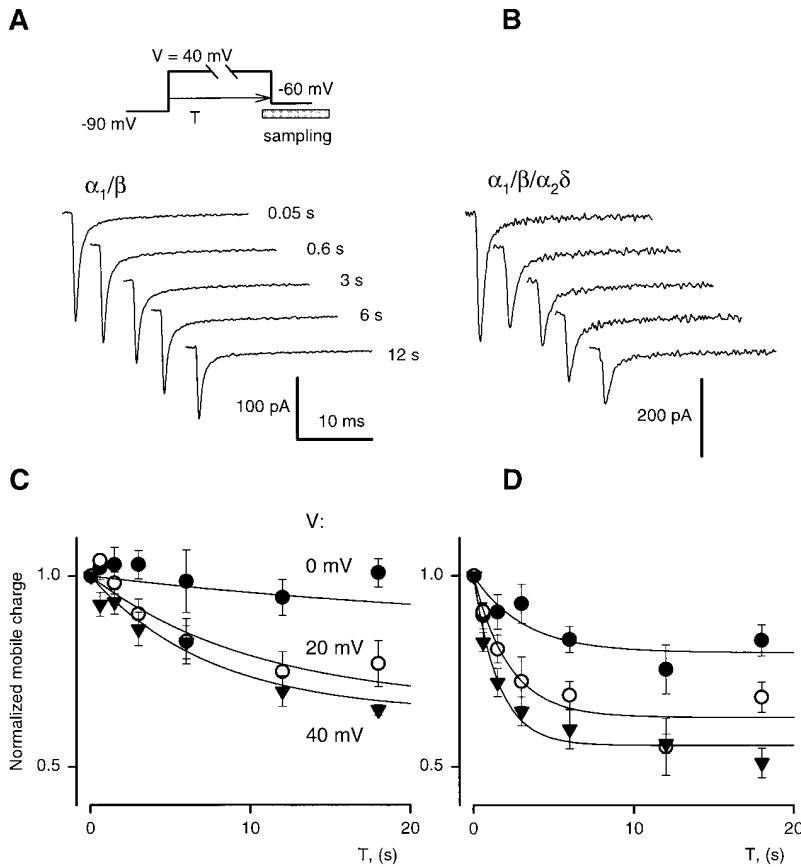


FIGURE 7. The $\alpha_2\delta$ subunit accelerates inactivation of gating currents. (A) OFF gating current transients in an α_1/β cell after different conditioning times at 40 mV. Conditioning times (T) are listed near each plot. (B) OFF gating current transients in an $\alpha_1/\beta/\alpha_2\delta$ cell after different times at 40 mV. (C) Charge transferred during the OFF transients plotted vs. T . Different symbols correspond to different values V , as listed. Charge transfers are normalized to the value after 0.05 s at the same V and averaged ($n = 6$ cells). Solid lines are best fits with the equation: $Q(T) = [1 - Q(\infty)] \exp(-T/\tau_{\text{ina}}) + Q(\infty)$. The best fit values of τ_{ina} are: 29.0 ± 13.0 s at 0 mV, 10.4 ± 2.6 s at 20 mV, and 7.5 ± 2.3 s at 40 mV. (D) Charge transfers with the same protocol as in C, for $\alpha_1/\beta/\alpha_2\delta$ cells ($n = 7$). The best fit values of τ_{ina} are: 3.2 ± 1.7 s at 0 mV, 2.2 ± 0.6 s at 20 mV, and 1.7 ± 0.3 s at 40 mV.

effect of the $\alpha_2\delta$ subunit on the onset kinetics of charge reduction. Charge movement was recorded during OFF transients from depolarizations of different duration (protocol at top). In α_1/β cells (Fig. 7 A), the OFF gating currents were progressively smaller for increasing test pulse durations up to 20 s. In cells with all three subunits (Fig. 7 B), reduction of the OFF transient saturated after 6 s of depolarization. To average and compare effects in different cells, values of charge moved after the long depolarizations were normalized to the value obtained from the transient after a 45-ms pulse to the same voltage. The averages are plotted in Fig. 7, C and D. Different symbols correspond to different pulse voltages. Reduction of the mobile charge was about three times faster in $\alpha_1/\beta/\alpha_2\delta$ cells for all voltages. The time constant of the reduction of gating charge at 40 mV in $\alpha_1/\beta/\alpha_2\delta$ cells was ~ 1.7 s, similar to that for the slow phase of Ba^{2+} current decay in these cells and in native cardiomyocytes.

We studied the effect of $\alpha_2\delta$ on recovery from inactivation applying a double pulse protocol often used with ionic currents. The experiment is illustrated in Fig. 8. After conditioning, the membrane was kept at the interpulse voltage for a variable time (T_{ip}), and then a test pulse to 50 mV was applied to assess charge movement. Reference test currents (Fig. 8, *thick traces*) were

recorded without conditioning. Gating currents elicited by test pulses from -60 mV took much longer to recover in $\alpha_1/\beta/\alpha_2\delta$ cells (Fig. 8 B) than in α_1/β cells (Fig. 8 A). As shown in Fig. 8, C and D, recovery from inactivation was substantially delayed by the $\alpha_2\delta$ subunit at every interpulse voltage tested.

In studies of recovery at very negative voltages, it was simpler to record the charge movement of inactivated channels (charge 2), which occurs at potentials negative to -50 mV. For this purpose, a test pulse to -50 mV was applied from an interpulse at more negative voltages (Fig. 9). Because inactivation involves a negative shift in the voltage dependence of charge movement, in the range negative to -50 mV, recovery is associated with a reduction in charge transfer. Given the conservation of total charge (Figs. 4–6), this should be accompanied by an equivalent increase of charge mobile in noninactivated channels (at potentials positive to -50 mV).

Independently of the presence of the $\alpha_2\delta$ subunit, conditioning caused an approximately twofold increase of charge transfer between -150 and -50 mV (Fig. 9, A and B), if recorded 50 ms after conditioning. Very little of this increase remained after 1 s at -150 mV in α_1/β cells, but $\sim 50\%$ persisted in $\alpha_1/\beta/\alpha_2\delta$ cells. Fig. 9, C and D, plot the increase of charge mobile between the interpulse voltage and -50 mV, normalized to the

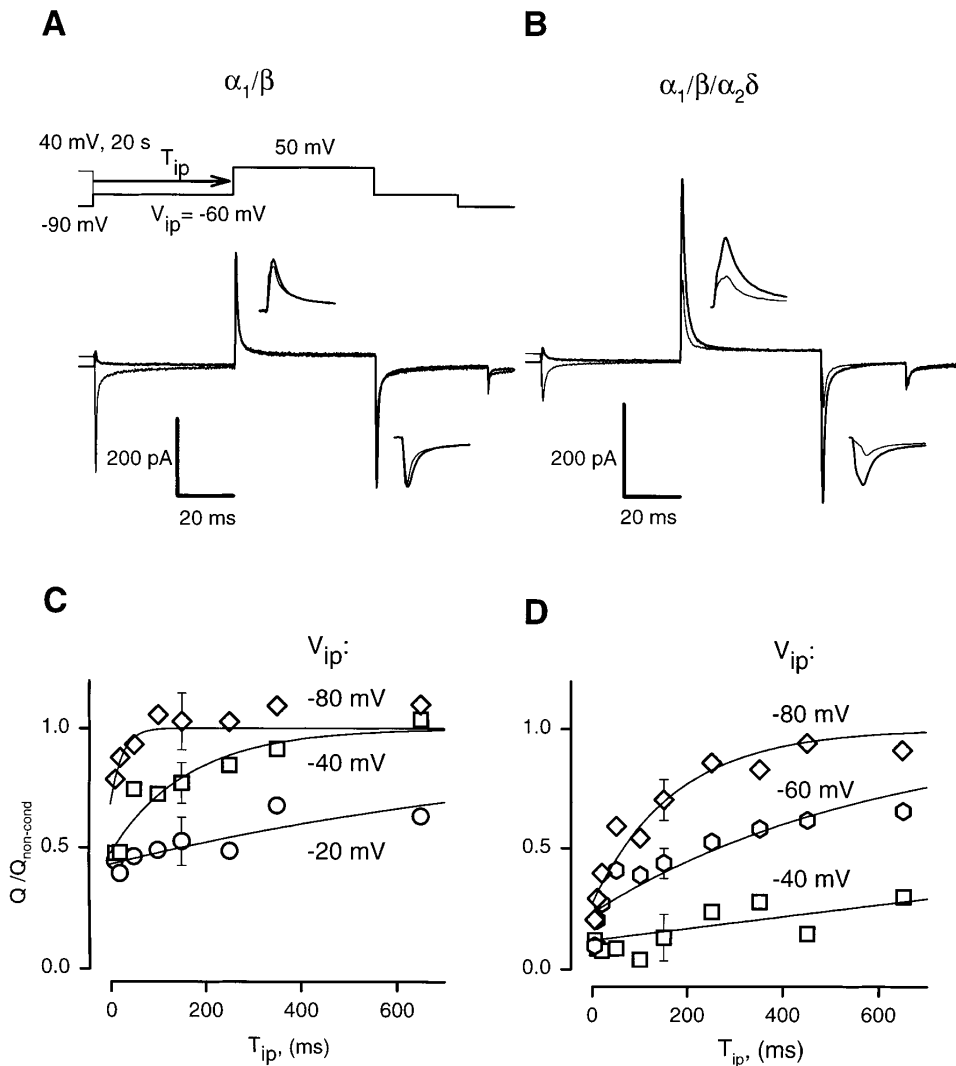


FIGURE 8. The $\alpha_2\delta$ subunit slows recovery of gating currents. (A) Gating currents elicited in an α_1/β cell by a test pulse to 50 mV from an interpulse of duration $T_{ip} = 50$ ms at voltage $V_{ip} = -60$ mV. Thick trace: reference, without conditioning. Thin trace: a 20-s long conditioning at 40 mV preceded the interpulse. Insets: same traces in an expanded time scale. (B) Same protocols as in A, for an $\alpha_1/\beta/\alpha_2\delta$ cell. (C) Relative charge mobile during ON transients such as those in A, plotted vs. T_{ip} . Different symbols correspond to different V_{ip} . Charge transfers were normalized to the value without conditioning in the same cell, and averaged ($n = 7$ cells). Solid lines are best fits with: $Q(T_{ip}) = 1 - [1 - Q(0)] \exp(-T_{ip}/\tau_r)$. The time constants τ_r are: 1.15 ± 0.31 s at -20 mV, 0.16 ± 0.04 s at -40 mV, and 0.04 ± 0.02 s at -80 mV. (D) Same as in C, for $\alpha_1/\beta/\alpha_2\delta$ cells ($n = 5$). τ_r is 2.47 ± 0.67 s at -40 mV, 0.61 ± 0.11 s at -60 mV, and 0.17 ± 0.03 s at -80 mV.

charge without conditioning, as a function of interpulse duration at -100 (\bullet), -150 (\circ), and -200 (\blacktriangle) mV for α_1/β and $\alpha_1/\beta/\alpha_2\delta$ cells, respectively. Curves are single exponential fits. Without the $\alpha_2\delta$ subunit, recovery kinetics were strongly voltage dependent in the range explored, and fastest at -200 mV ($\tau \approx 300$ ms). In contrast, with the $\alpha_2\delta$ subunit recovery was slow ($\tau \approx 2$ s) and weakly voltage dependent in this range. The ancillary subunit not only slows the recovery process but also insulates it from the influence of voltage.

DISCUSSION

Modal Interconversion of Intramembrane Charge Movement during Inactivation of α_{1C} Channels

The main finding of this study is that voltage-dependent inactivation of heterologously expressed cardiac Ca channels is associated with a large negative shift in

the voltage dependence of their charge movement. The intramembrane charge movement in inactivated α_1/β channels has a transition potential of ~ -90 mV, which is the same as in native L-type Ca channels (Brum and Ríos, 1987; Shirokov et al., 1992). The charge remains mobile at these voltages until channels recover from inactivation, a first order process with a time constant of ~ 300 ms at -200 mV. Because the time scale of charge movement in inactivated α_1/β channels ($\tau \leq 15$ ms) is much faster than recovery from inactivation, the expressed channels exhibit a separate inactivated mode, and the term charge 2 can be applied to the charge mobile at negative voltages in inactivated channels. With $\alpha_1/\beta/\alpha_2\delta$ channels, the modal separation is even more clear cut.

We showed previously that the onset of inactivation of gating currents in α_1/β cells is parallel to a slow phase of Ba^{2+} current decay ($\tau \approx 8$ s), and that addition of the $\alpha_2\delta$ subunit increases the slow rate of ionic current decay, making it similar to that in cardiac cells

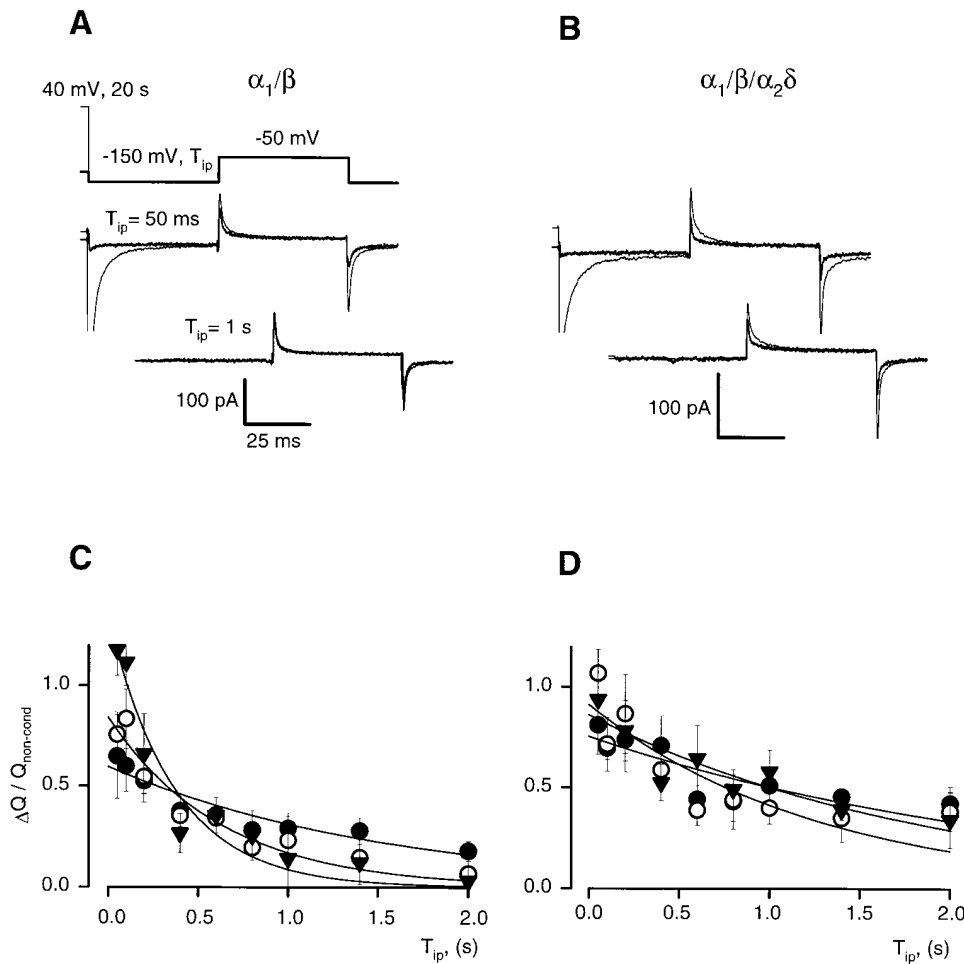


FIGURE 9. The $\alpha_2\delta$ subunit slows reduction of charge mobile at negative voltages. (A) Charge movement currents elicited in an α_1/β cell by a test pulse to -50 mV from an interpulse of $T_{ip} = 50$ ms at $V_{ip} = -150$ mV. (*thick trace*) Reference. (*thin trace*) After a 20-s long conditioning at 40 mV. (B) Same protocols as in A, for an $\alpha_1/\beta/\alpha_2\delta$ cell. (C) Relative increase of charge mobile during ON transients such as those in A, plotted vs. T_{ip} . Different symbols correspond to different V_{ip} . Each increase in charge transfer was normalized to the charge transfer in reference and averaged ($n = 4$ cells). Solid lines are best fits with: $Q(T_{ip}) = Q(0) \exp(-T_{ip}/\tau)$. τ is 1.30 ± 0.19 s at -100 mV, 0.52 ± 0.09 s at -150 mV, and 0.32 ± 0.06 s at -200 mV. (D) Same as in C, for $\alpha_1/\beta/\alpha_2\delta$ cells ($n = 4$). τ at -100 mV is 2.46 ± 0.63 s, at -150 mV is 1.66 ± 0.53 s, and at -200 mV is 1.87 ± 0.40 s.

($\tau \approx 2$ s; Ferreira et al., 1997). In agreement with these earlier observations, we now find a time constant of ~ 2 s for the reduction of gating currents upon inactivation in cells expressing all three subunits (Fig. 7). Working with native cells at room temperature, we estimated the onset τ of charge interconversion at ≈ 0.6 s (Shirokov et al., 1993). This estimate may be at fault because of the unavoidable contribution of Na channels to the native gating currents. A discrepancy in the same direction exists for the time course of recovery from inactivation of gating charge (charge 1) in native cells. We reported a time constant of 200 ms for this process (Shirokov et al., 1992), while in the present measurements with expressed channels containing the $\alpha_2\delta$ subunit $\tau \approx 1.5$ s (Fig. 9). Again, and for the same reasons, the present measurements must be considered more reliable. Interestingly, in native skeletal muscle, recovery of charge 1 is much slower ($\tau \approx 3$ s; Brum and Ríos, 1987). The discrepancy in results in native cells could reflect structural differences between the two channels. It could also reflect a better determination, given the vast predominance of dihydropyridine receptors over other sources of intramembranous charge movement in skeletal muscle.

Biophysical Effects of the $\alpha_2\delta$ Subunit

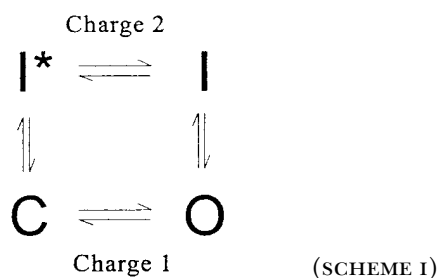
The present results demonstrate that the $\alpha_2\delta$ subunit promotes inactivation of gating currents in cardiac L-type Ca channels. We found that the $\alpha_2\delta$ subunit made the onset of inactivation of intramembrane charge movement three to four times faster, and the recovery from inactivation about five times slower. On the other hand, inactivation of gating currents in L-type Ca channels was much slower than activation gating, even in the presence of the $\alpha_2\delta$ subunit ($\tau \approx 2$ s). It is therefore unlikely that the increased rate of inactivation results from primary changes in activation.

In spite of profound effects of the $\alpha_2\delta$ subunit on inactivation kinetics, the voltage dependence of charge movement in primed and inactivated channels was not significantly changed. In agreement with previous findings (Singer et al., 1991; Welling et al., 1993; Shistik et al., 1995; Bangalore et al., 1996), we found little effect of the $\alpha_2\delta$ subunit on voltage dependence of activation of ionic currents on α_1/β cells (data not shown). In contrast, Felix et al. (1997) reported that the $\alpha_2\delta$ subunit, added to the α_{1C} in the absence of the β subunit,

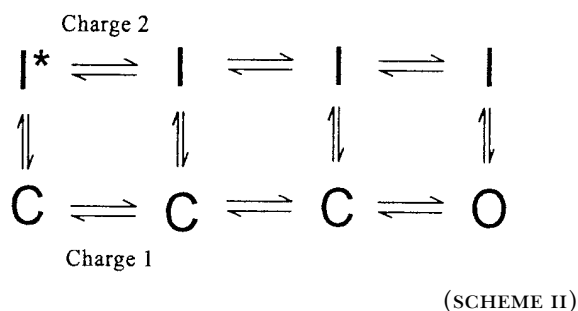
shifted the activation of ionic currents in tsA201 cells by ~ -10 mV. In *Xenopus* oocytes, coexpression of $\alpha_2\delta$ and α_1 subunits increased single channel open probability (Shistik et al., 1995), while in HEK 293 cells addition of $\alpha_2\delta$ to α_1 and β subunits speeded up activation and deactivation (Bangalore et al., 1996).

As shown previously (reviewed by Gurnett and Campbell, 1996), the $\alpha_2\delta$ subunit shifts by ~ -10 mV the steady state inactivation curves of recombinant Ca channels. In light of these observations, our finding that the charge distributions in inactivated channels are unaffected by the $\alpha_2\delta$ subunit may seem surprising. This and other aspects, however, may be accounted for with biophysical models of voltage-dependent inactivation.

Inactivation of gating currents in Ca channels has been represented by a minimal four state diagram (Scheme I). In it, the "horizontal" transitions are fast and voltage dependent, while (voltage-independent) "vertical" transitions are much slower, which qualifies the pairs of states, C, O, and I^* , I, as separate modes that account, respectively, for charge 1 and charge 2. The model is "allosteric": inactivation and activation occur at separate sites, as the movement of separate gates that influence each other but move individually.



This model already has most of the observed properties, and accommodates the effect of $\alpha_2\delta$, which could simply be represented by an equal reduction in the free energy of states I and I^* and a decrease in the energy barrier between O and I. It is, however, too oversimplified, failing to account for charge movement between and inactivation from closed states.

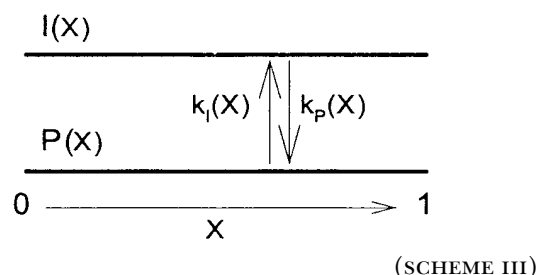


Scheme II represents a generalization of the allosteric model (Marks and Jones, 1992; Kuo and Bean

1994; Olcese et al., 1997), in which activation gating is represented as a multi-step reaction, and inactivation is likely to occur from closed states.

Scheme II also features charge 1 and charge 2 modes, an aspect used recently by Olcese et al. (1997) to represent similar observations on gating currents of *Shaker* K channels. However, it has many parameters that cannot be constrained, especially the number of closed states. For this reason, we generalized these models by incorporating continuum activation gating (Millhauser et al., 1988; Lauger, 1988) in a version of Levitt (1989). This simplified the kinetic scheme, reduced the number of parameters, and gave a more intuitive view of the gating process.

The model equations are presented in detail in the APPENDIX. Inactivation is described as a voltage-independent reaction, of rate constants k_p and k_i , between two modes of the channel: P (primed) and I (inactivated). The gating process associated with intramembrane charge movement is represented by a conformational movement along a reaction coordinate x , driven by the electric field (Scheme III). Because there are no free energy barriers, the movement is continuous, akin to diffusion. The generalized reaction coordinate projects to one dimension the set of conformations accessible to the channel. A given value of the coordinate characterizes all conformations that take the same amount of energy from the electric field.



The state of the ensemble of channels is described by two probability density functions, $P(x)$ and $I(x)$. Evolution of these functions is determined by diffusion reaction within the free energy profiles $U_p(x)$ and $U_i(x)$, which have chemical and electrical additive components. As stated above, at any given transmembrane voltage the electrical energy term will vary linearly with x . An additional assumption, primarily made for simplicity, is that the chemical free energy also depends linearly on x . Therefore, the joint dependence of U_p (or U_i) on x and V is represented by ruled surfaces (hyperboloids), as in Fig. 10, where the parameters are chosen to simulate data in the presence of $\alpha_2\delta$.

To reproduce the tendency to inactivation at positive and recovery at negative voltages, $U_p(x)$ and $U_i(x)$ must cross, so that P is favored at the values of x near 0, which are populated at the resting potential, and the

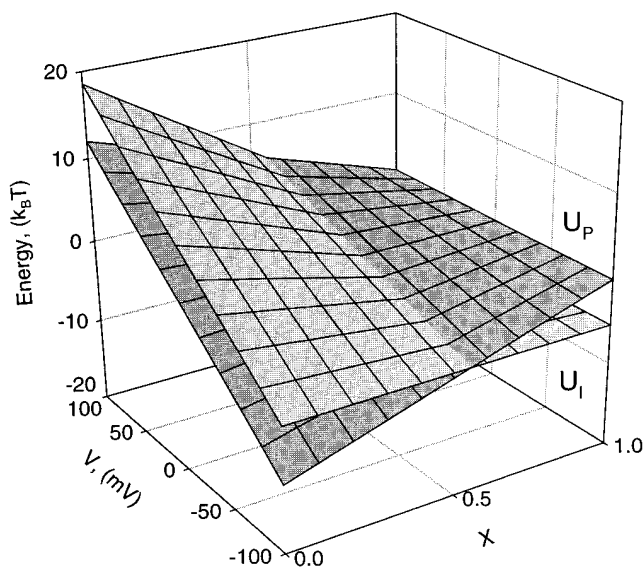


FIGURE 10. Free energy profiles of the continuum model. Energies U_P and U_I of the primed and inactivated modes in the model, given by Eq. 3 (APPENDIX), plotted as a function of transmembrane voltage V and conformational coordinate x . Parameter χ (the value of x at which the planes intersect) is set to 0.55, the value used to simulate the presence of $\alpha_2\delta$.

opposite occurs at x near 1. Because intermodal transitions are assumed to be intrinsically voltage independent, the transfer of charge as a function of x must be the same in the two modes, or, equivalently, $\partial U_P/\partial V = \partial U_I/\partial V$. Because voltage cannot directly alter intermodal distribution, the value of x at which P and I are equally probable (intersection of the planes $U_P(x,V)$ and $U_I(x,V)$ in Fig. 10) will be a constant, χ , independent of V . The continuum model requires four thermodynamic parameters and three kinetic parameters, fewer than even the simple state model of Scheme I.

At equilibrium, the distributions satisfy:

$$P_\infty(x,V) \propto e^{-U_P(x,V)}, \text{ and } I_\infty(x,V) \propto e^{-U_I(x,V)}. \quad (2)$$

Therefore, in channels held near resting voltages, $P_\infty(x,V)$ is large at x close to 0, while $I_\infty(x,V)$ is very small. When the voltage is positive, $P_\infty(x,V)$ becomes small for all x , while $I_\infty(x,V)$ is high at x close to 1. Fig. 11 illustrates the evolution of the system [$P(x,t)$ and $I(x,t)$] during a pulse from -100 to 0 mV. The initial conditions $P(x,0)$ and $I(x,0)$ were calculated as the equilibrium distributions at -100 mV. The voltage was changed to 0 mV with exponential time course ($\tau_m = 0.2$ ms). The system evolved with two widely separated time scales, one associated with movements along x and the other with the inactivation transition. The fast process is illustrated in Fig. 11, *top*. A and B plot $P(x,t)$ and $I(x,t)$ during the first 5 ms of the voltage step. Both $P(x,t)$ and $I(x,t)$ redistribute towards $x = 1$, reaching a

quasi stationary situation, and generating measurable charge movement associated with diffusion along x (Fig. 11 C). After the quasi steady state is reached, probability densities continue to change at a slow rate determined by the inactivation reaction. Fig. 11, *bottom*, illustrates this slow process. The marked complementary changes in total occupancy of modes P and I (Fig. 11 F) are accompanied by additional diffusion along x . The resulting charge movements are undetectable because of their slow rate, limited by the inactivation reaction. This additional redistribution of charge can be estimated as the difference between steady state charge transfer, calculated from the equilibrium distributions (P_∞ and I_∞), and charge transfer determined by numerical integration of the simulated current, as if it were an experimental record.

Fig. 12 illustrates the comparison. Gating currents simulated with pulses from -200 mV are shown in Fig. 12 A, *left*. The areas under ON transients are shown in Fig. 12 B, ●. The recordable charge transfer for steps from -200 mV occurs at more positive voltages than the equilibrium distribution of charge $Q_{eq}(V)$ (Fig. 12, *curve*). The vertical difference between the curve and the symbols corresponds to the additional transfer that occurs slowly as channels inactivate.

Similarly, when pulses are applied from 200 mV, charge mobile in the fast time domain corresponds to redistribution of channels in mode I along the x axis, and the charge transfer (Fig. 12 B, ○) occurs at more negative voltages. Corresponding intramembrane charge movement currents are shown in Fig. 12 A, *right*.

The steepness of the Boltzmann fits to the simulated charge transfer was ~ 25 mV in both primed and fully inactivated channels, corresponding to the transfer of one elementary charge in a single step transition. With the continuum model, the maximal charge transfer had to be set to three elementary charges to simulate such shallow distributions. Interestingly, model-independent estimates of maximal unitary gating charge from gating current noise of Na and K channels provided similar values. 2.4 elementary charges were required assuming that the gating current noise is produced by a number of independent identical particles, which during activation undergo a single irreversible transition (Conti and Stühmer, 1989; Sigg et al., 1994). The continuum model therefore reconciles estimates of elementary charge from microscopic and macroscopic gating current measurements, provided that the macroscopic charge movement is generated by particles with approximately three elementary charges moving independently and with the same half-activation potential. Because 8–12 elementary charges transfer during channel activation, ~ 4 such independent particles would be required for channel opening. This would be the case, for example, if the movement of individual S4

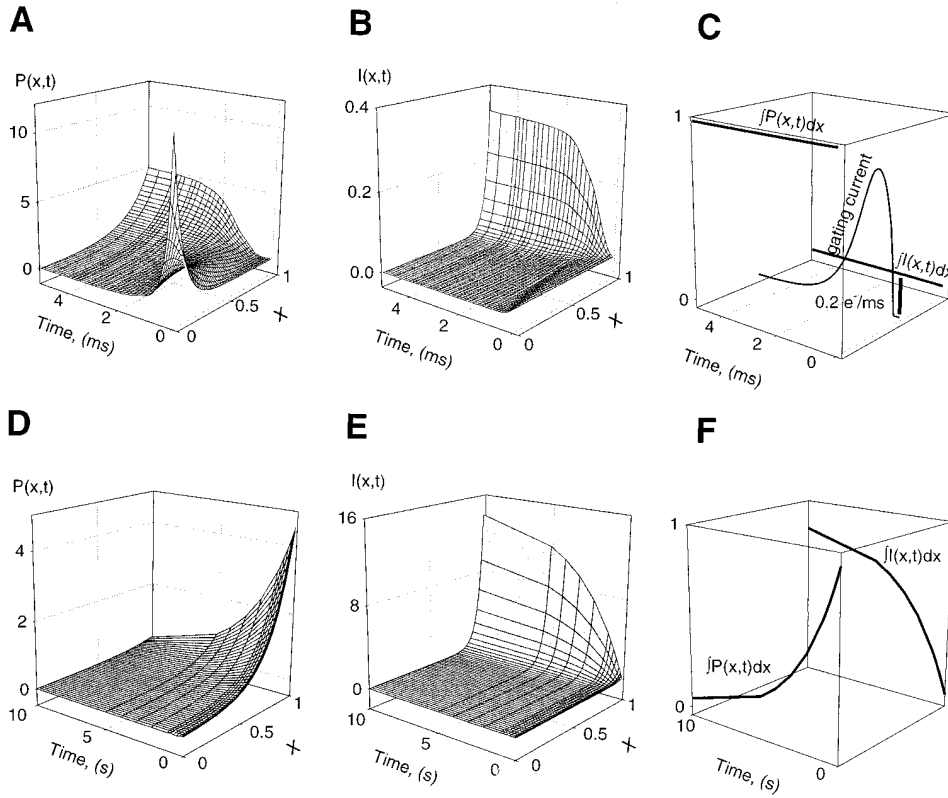


FIGURE 11. Two time domains of inactivation. (A) Initial evolution $P(x,t)$ of the (probability density in the) primed mode, in response to a pulse to 0 mV from a holding potential of -100 mV. (B) Corresponding evolution $I(x,t)$ of the inactivated mode. (C, *thin line*) Gating currents generated during the pulse. (*thick lines*) Total modal probabilities, calculated as integrals over x of P and I . Note that the modal probabilities change little during the interval of measurable gating current. (D and E) $P(x,t)$ and $I(x,t)$ in response to the same pulse on a longer time scale (0.05–10 s). (F) Total modal probabilities on the same time scale.

segments occurred independently and over the same voltage range, and if all four segments had to move to cause activation.

Charge distributions of squid axon Na, skeletal muscle Ca, and *Shaker* K channels are less steep after moderate inactivation (Bezanilla et al., 1982; Brum and Ríos, 1987; Olcese et al., 1997). The observation also applied for moderately inactivated cardiac Ca channels in the present work (data not shown). Model simulations of this condition are illustrated in Fig. 12 C. The thick curves are simulated charge distributions in primed and inactivated channels (spline curves through Fig. 12 B, \circ and \bullet). The dark gray curve simulates with the continuum model the measurable charge transfer upon application of negative-going pulses after a 1-s conditioning at 200 mV. In contrast, the four-state model of Scheme I² generated the two-sigmoidal distribution

²Parameters of the four-state charge 1–charge 2 model (see Scheme I) were:

$$\begin{aligned}
 k_{C,O} &= 0.5 e^{\left(\frac{V}{16}\right)}, & k_{O,C} &= 0.5 e^{\left(\frac{V}{16}\right)}, \\
 k_{I^*,I} &= 0.05 e^{\left(\frac{100+V}{16}\right)}, & k_{I,I^*} &= 0.05 e^{\left(\frac{-100-V}{16}\right)}, \\
 k_{O,I} &= 0.0005, & k_{I,O} &= 0.00005, \\
 k_{I^*,C} + k_{C,I^*} &= 0.001, & \frac{k_{C,I^*}}{k_{I^*,C}} &= e^{\left(\frac{-100}{8}\right)},
 \end{aligned}$$

where rate constants are in ms^{-1} and V is in millivolts.

plotted in thin trace, which is close to a linear combination of the fully primed and fully inactivated distributions. Such sharp separation of sigmoidal components was never observed experimentally. Even though the two-modal distributions of charge could be isolated experimentally in the presence of $\alpha_2\delta$, the distribution in partially inactivated conditions was not a linear combination of the modal distributions. This is well reproduced by the continuum model.

Simulation of the Effect of the $\alpha_2\delta$ Subunit

To model the effects of the $\alpha_2\delta$ subunit on voltage-dependent inactivation, we had only to assume that the subunit stabilizes the inactivated mode I. We specifically assumed that it makes the energy difference between I and P more negative at all values of x . Because of the linearity of $U_1(x,V)$, this is equivalent to a decrease in χ , the x value of half inactivation. While inactivation of α_1/β channels was simulated with $\chi = 0.8$, $\alpha_1/\beta/\alpha_2\delta$ channels required $\chi = 0.55$ as sole parameter change. The simulated charge distributions of primed and inactivated channels are in Fig. 13. In correspondence with experimental observations (Table I), the transition potentials of simulated charge distributions in fully primed or fully inactivated channels were not affected by the change in χ . (The reason is simple: the voltage distribution of mobile charge within modes is sensitive to the chemical potential gradient, not to an additive constant.) The model also described well the

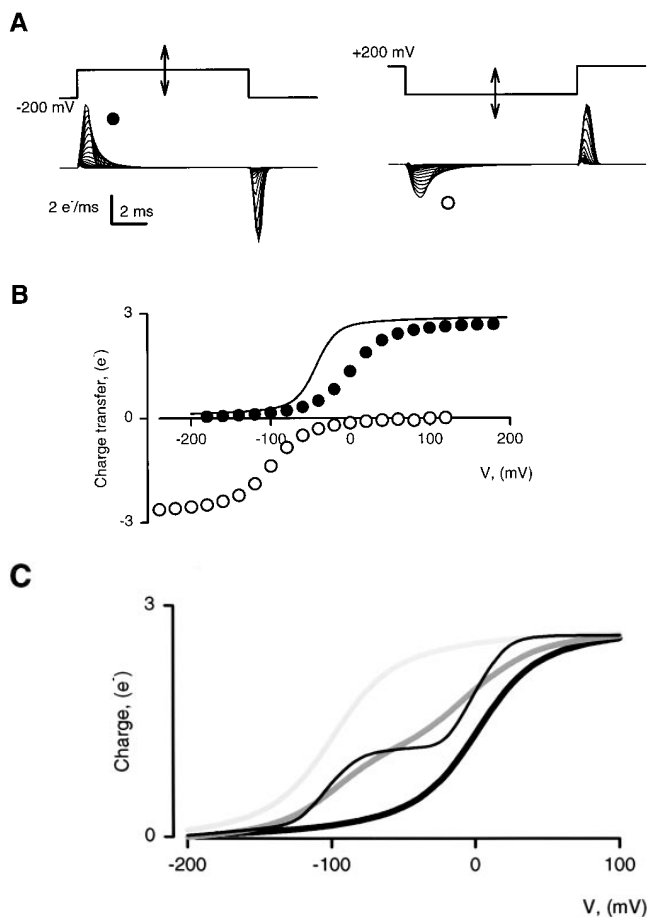


FIGURE 12. Simulated charge transfers at two holding potentials. (A, left) Gating currents elicited by pulses from -200 mV to different voltages (V). (right) Gating currents from 200 mV. (B) Charge transferred in records in A vs. V. (●) Charge transfer from -200 mV. (○) Charge transfer from 200 mV. (solid line) Equilibrium charge distribution as a function of holding potential. (C) Charge distribution curves, splines through the points in B shifted vertically as described in the text. (thick black line) Distribution at holding potential -200 mV. (thick light grey line) Distribution at holding potential 200 mV. (thick dark grey line) Charge distribution after a 1-s conditioning pulse from -200 to 200 mV, which makes the two modal probabilities approximately equal (0.5). (thin line) Charge distribution generated by Scheme I after the 1-s conditioning pulse from -200 to 200 mV, with parameters chosen to best reproduce the behavior of the continuum model (see DISCUSSION).

observed difference in the steepness of the charge distributions between primed and conditioned α_1/β channels. In conditioned α_1/β cells, the steepness of charge distribution measured from an interpulse at 40 mV was ~ 40 mV, whereas in nonconditioned cells (-150 mV interpulse) it was ~ 30 mV. In conditions simulating α_1/β channels ($\chi = 0.8$), the charge distribution of the inactivated channels was also shallower (33 mV) than that of noninactivated channels (25 mV). The difference between the steepness of charge distribution in primed and inactivated α_1/β channels is due to the fact that, because of their fast rate of recovery, the charge

distribution of inactivated α_1/β channels cannot be isolated experimentally.

The onset kinetics of inactivation in the model were assessed with the pulse protocol used in the experiment of Fig. 7. The corresponding simulated dependencies of amounts of charge movements on the duration of conditioning depolarization are shown in Fig. 13, C and D. Reduction of charge mobile above -50 mV was more rapid for $\chi = 0.55$ (simulating channels with $\alpha_2\delta$) than for $\chi = 0.8$, giving rates similar to those obtained experimentally.

Recovery properties of the model were studied with pulse protocols similar to those illustrated in Fig. 9. Fig. 9, E and F, show dependencies of the amount of charge mobile below -50 mV on the interpulse duration. As observed in the experiments with $\alpha_1/\beta/\alpha_2\delta$ (Fig. 9 D), simulations with $\chi = 0.55$ (Fig. 13 F) exhibit a slow recovery rate and are weakly voltage dependent at voltages below -150 mV. In agreement with the observations in α_1/β cells (Fig. 9 C), with $\chi = 0.8$ recovery is three to five times faster (Fig. 13 E), approaching the speed of recordable charge movement. In all, the continuum model reproduces well the effects of $\alpha_2\delta$, under the hypothesis that the subunit changes a single parameter of energy distribution.

Modal Separation

With $\chi = 0.55$, the model behaves similarly to the channels in the presence of $\alpha_2\delta$, evolving with two well-defined time scales: a fast one associated with measurable charge movement and a slow one determined by inactivation. This separation of time scales is a requisite for a well-defined charge 2, which can be ascribed unequivocally to mode I.

When χ is close to 1 (simulating the absence of the $\alpha_2\delta$ subunit) the $I \leftrightarrow P$ conversion becomes very fast at negative voltages, and the separation between time scales becomes less clear cut. At -200 mV, the most negative potential that is consistently accessible, recovery in simulations of channels lacking $\alpha_2\delta$ has a $\tau = 0.28$ s (Fig. 13 E), in good agreement with the experiment (0.32 s, Fig. 9 C), and well beyond the time needed to complete the measurable movement of charge (~ 50 ms). The fastest possible recovery is achieved from $x = 0$ (a condition that requires forbiddingly large negative potentials) and proceeds with a time constant of ~ 0.16 s. This is close to but greater than the time of charge movement, so that modal separation still prevails in simulations of channels without $\alpha_2\delta$, even at experimentally inaccessible negative potentials.

If the rate constant of the $I \leftrightarrow P$ reaction (see APPENDIX, Eq. 11) was just an order of magnitude greater than the value determined for channels without the $\alpha_2\delta$ subunit, modal separation would break down. This would be reflected in the appearance of a substantial slow component in the charge movement during recovery.

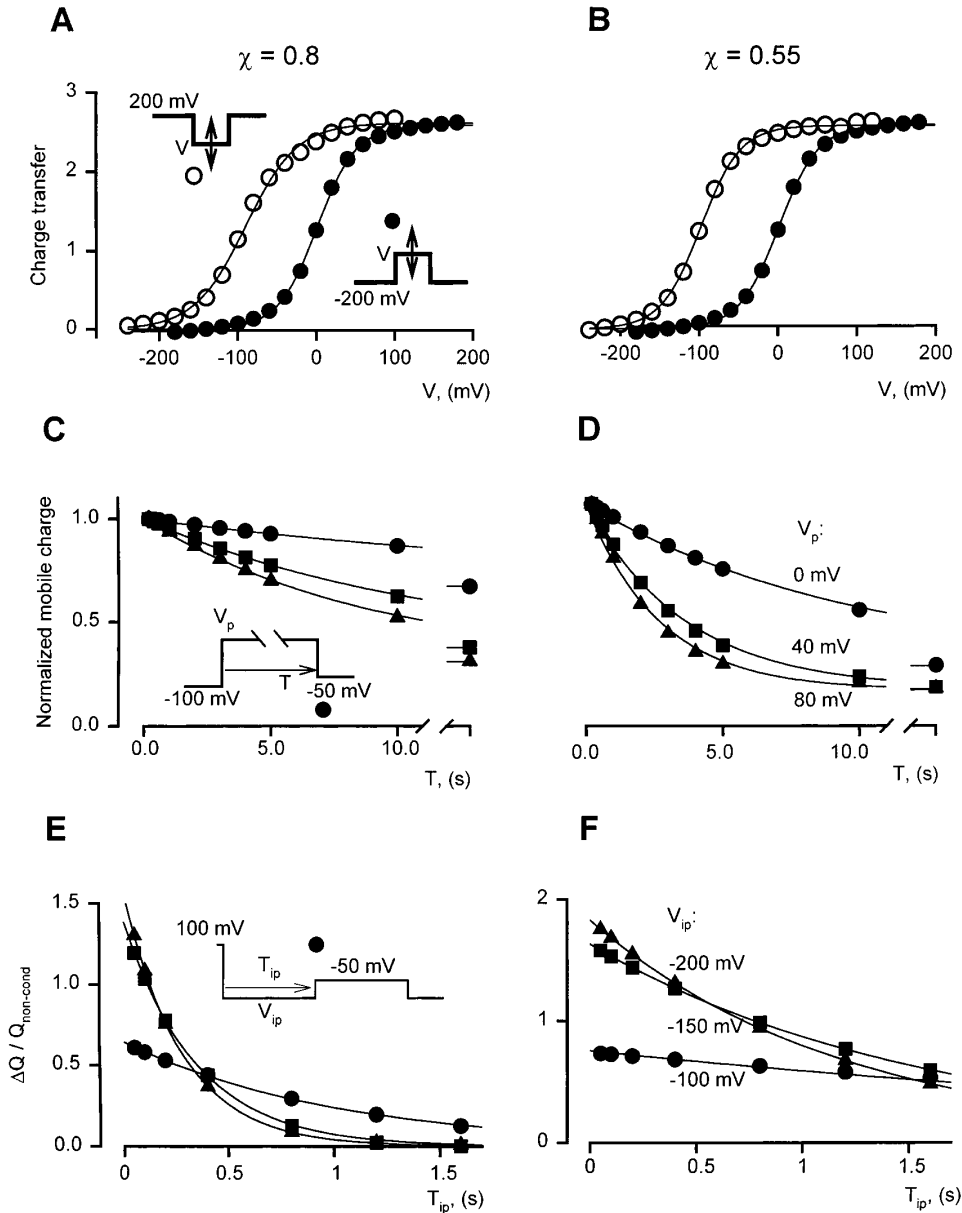


FIGURE 13. Simulation of the effect of $\alpha_2\delta$ on inactivation of gating currents. (A) Charge distributions, obtained as described for Fig. 12 with pulse patterns illustrated, simulating primed (○) or inactivated α_1/β channels ($\chi = 0.8$). The lines represent Boltzmann fits with the following parameters: for primed channels $Q_{\text{MAX}} = 2.6 e^-$, $V_{1/2} = 0.9 \text{ mV}$, $K = 25.1 \text{ mV}$. For inactivated channels, $Q_{\text{MAX}} = 2.6 e^-$, $V_{1/2} = -90.5 \text{ mV}$, $K = 32.7 \text{ mV}$. Comparable experimental data are in Fig. 5 A. (B) Same as in A, with $\chi = 0.55$, to simulate $\alpha_1/\beta/\alpha_2\delta$ channels. For primed channels, $Q_{\text{MAX}} = 2.6 e^-$, $V_{1/2} = 0.8 \text{ mV}$, $K = 25.2 \text{ mV}$. For inactivated channels, $Q_{\text{MAX}} = 2.6 e^-$, $V_{1/2} = -98.3 \text{ mV}$, $K = 25.3 \text{ mV}$. Comparable experimental data are in Fig. 5 B. (C) Onset of reduction of simulated gating currents upon conditioning to three different voltages V_p in α_1/β simulations. The fits are given by $Q(t) = 1 - [1 - Q(\infty)] \exp(-t/\tau)$. Values of fit parameters [$Q(\infty)$ and τ] are: 0.67 and 20.01 s for $V_p = 0 \text{ mV}$, 0.38 and 11.12 s for 40 mV, 0.31 and 8.85 s for 80 mV. Comparable experimental data are in Fig. 7 C. (D) Onset of reduction of gating currents in $\alpha_1/\beta/\alpha_2\delta$ simulations. Values of fit parameters [$Q(\infty)$ and τ] are: 0.27 and 9.78 s for $V_p = 0 \text{ mV}$, 0.17 and 3.61 s for 40 mV, 0.16 and 2.68 s for 80 mV. Experimental data are in Fig. 7 D. (E) Recovery from reduction of charge movement in α_1/β simulations at three different inter-pulse voltages V_{ip} . The fits are generated with $Q(t) = Q(\chi) \exp(-t/\tau)$. Corresponding pa-

rameters [$Q(0)$ and τ] are: 0.64 and 1.00 s for $V_{ip} = -100 \text{ mV}$; 1.39 and 0.341 s for -150 mV ; 1.56 and 0.275 s for -200 mV . Experimental data are in Fig. 9 C. (F) Recovery in $\alpha_1/\beta/\alpha_2\delta$ simulations. Values of fit parameters [$Q(\infty)$ and τ] are: 0.75 and 3.96 s for $V_{ip} = -100 \text{ mV}$; 1.63 and 1.58 s for -150 mV ; 1.83 and 1.20 s for -200 mV . Experimental data are in Fig. 9 D.

ery at intermediate negative voltages, cotemporal with $I \rightarrow P$ transitions. Such a component, not observed experimentally in Ca channels, is a distinctive feature of the gating current in Na channels, the “remobilization” component observed when channels are reprimed at -130 mV (Armstrong and Bezanilla, 1977). For the continuum model to simulate such fast inactivation, it is necessary that the inactivation processes further stabilize the mobile charged moieties in the *trans* (open) position. In that case, some values of x close to 0 will not be populated in the inactivated mode at intermedi-

ate negative voltages.

Likewise, Kuo and Bean (1994) were able to simulate onset and recovery of fast inactivation in Na channels with the model illustrated by Scheme II. Therefore, both modal interconversion, documented in the present work, and the so-called charge immobilization phenomena that accompany fast inactivation can be reproduced with general allosteric models of the types represented by Schemes II and III.

The preceding considerations are relevant to whether voltage-dependent inactivation in L-type Ca channels is

slow (C-type) or fast (N-type). Inactivation appears to be slow because it exhibits clear modal separation.

On the other hand, there is an important distinction between voltage-dependent inactivation of Ca channels and slow inactivation of Na and K channels. Whereas in these channels recovery from slow inactivation takes many seconds, in L-type Ca channels recovery would be fast, were it not for the stabilizing effect of the $\alpha_2\delta$ subunit on the voltage-inactivated states. Structure-function studies are required for establishing the mechanism of this stabilization.

APPENDIX

The continuum model of inactivation, represented in Scheme III, comprises the following set of equations. The energies of modes P and I, in dimensionless expressions are:

$$\begin{aligned} U_P &= q(v - v_p)(1 - x) = A(1 - x) + n_g v(1 - x), \text{ and} \\ U_I &= q(v - v_l)(1 - x) + \epsilon_{IP} = U_P + C(1 - x - B), \end{aligned} \quad (3)$$

where $q = Q/e$ is the total charge transfer (in number of electrons), v is dimensionless voltage, equal to $Ve/k_B T$, v_p and v_l are the transition potentials of the corresponding modes, ϵ_{IP} is the energy difference between U_I and U_P at $x = 1$, and A , B , C , and n_g are constants (Levitt, 1989).

To emphasize that at $x = \chi \equiv 1 - B$ the energy difference U_{IP} changes its sign, Eq. 3 can be rewritten as

$$\begin{aligned} U_{IP} &= \epsilon_{IP} + C(1 - x) = C(1 - B - x) \\ &= q(v_p - v_l)(\chi - x). \end{aligned} \quad (4)$$

The steady state probability densities are defined as follows:

$$\begin{aligned} P_\infty(x, v) &= \frac{1}{S} e^{-U_P(x, v)}, \quad I_\infty(x, v) = \frac{1}{S} e^{-U_I(x, v)}, \\ \text{where } S &= \int_0^1 (e^{-U_P(x, v)} + e^{-U_I(x, v)}) dx. \end{aligned} \quad (5)$$

The steady state charge distribution $Q_{eq}(V)$ is calculated numerically from

$$Q_{eq}(v) = \int_0^1 q [P_\infty(x, v) + I_\infty(x, v)] x dx. \quad (6)$$

Transitions between the two modes are described by the following set of differential equations:

$$\begin{aligned} \frac{\partial P}{\partial t} &= -\frac{\partial J_P}{\partial x} + k_p I - k_l P, \\ J_P &= -D_P \left(\frac{\partial P}{\partial x} + P \frac{dU_P}{dx} \right), \text{ and} \\ \frac{\partial I}{\partial t} &= -D_I \frac{\partial J_I}{\partial x} + k_l P - k_p I, \\ J_I &= -D_I \left(\frac{\partial I}{\partial x} + I \frac{dU_I}{dx} \right), \end{aligned} \quad (7)$$

where D_P and D_I are generalized diffusion coefficients. The fluxes satisfy reflective boundary conditions:

$$J_P(0) = J_I(0) = J_P(1) = J_I(1) = 0. \quad (8)$$

The rate constants of the interconversion are defined by the energy profiles. For a symmetrical barrier, the rates are

$$k_p = k_0 e^{\frac{U_{IP}}{2}}, \text{ and } k_l = k_0 e^{-\frac{U_{IP}}{2}}. \quad (9)$$

Eqs. 7 and 8 were solved using a fully implicit finite differencing scheme with a band diagonal system of linear equations. The band diagonal system was solved by the *bandc* and *bandks* routines of Press et al. (1992) (The computer program for simulation [DOS and X-Win versions] can be obtained by e-mail request to rshiroko@rush.edu). The x grade was 50. The time steps were automatically adjustable depending on accuracy of solution. The accuracy of the solution was determined as deviation of the total probability from 1 and it was set at 3%. For simulations we used: $q = 3$, $v_p = 0$, $v_l = -4$ (equivalent to -100 mV at room temperature), $D_P = 100 \text{ s}^{-1}$, $D_I = 50 \text{ s}^{-1}$, $k_0 = 0.05 \text{ s}^{-1}$, and $\chi = 0.8$ for α_1/β channels or $\chi = 0.55$ for $\alpha_1/\beta/\alpha_2\delta$ channels.

The transfer of mobile charge (from an all-in starting distribution) is calculated by

$$Q(t) = \int_0^1 q [P(x, t) + I(x, t)] x dx, \quad (10)$$

consistent with the definition of the potentials (Eq. 3). The charge movement current is $i_g(t) = dQ/dt$.

From Eqs. 4 and 9, the time constant of the $I \leftrightarrow P$ transition (τ_{IP}) is limited by

$$\tau_{IP}(x) \equiv (k_l + k_p)^{-1} \approx k_0^{-1} e^{-q(v_p - v_l) \frac{(\chi - x)}{2}}, \quad (11)$$

or $\ln(\tau_{IP} k_0) \approx -6(\chi - x)$ for the parameters used. Because the difference between v_p and v_l is substantial, the time constant τ_{IP} is small compared with k_0 , when χ is close to 1 and at x is close to 0.

We thank Drs. Duanpin Chen (Rush University) for discussions and help with the continuum model, and Werner Melzer (University of Ulm, Ulm, Germany) for many comments on the manuscript.

This work was supported by a Scientist Development Grant from the American Heart Association (to R. Shirokov) and by National Institutes of Health grant AR-43113 (to E. Ríos).

Original version received 8 January 1998 and accepted version received 23 March 1998.

REFERENCES

- Armstrong, C.M., and F. Bezanilla. 1977. Inactivation of the sodium channel. II. Gating current experiments. *J. Gen. Physiol.* 70:567–590.
- Bangalore, R., G. Mehrke, K. Gingrich, F. Hofmann, and R.S. Kass. 1996. Influence of L-type Ca channel $\alpha_2\delta$ subunit on ionic and gating current in transiently transfected HEK 293 cells. *Am. J. Physiol.* 270:H1521–H1528.
- Balsler, J.R., H.B. Nuss, D. Romashko, E. Marban, and G.T. Tomaselli. 1996. Functional consequences of lidocaine binding to slow-inactivated sodium channels. *J. Gen. Physiol.* 107:643–658.
- Bezanilla, F., R.E. Taylor, and J. Fernandez. 1982. Distribution and kinetics of membrane dielectric polarization. I. Long-term inactivation of gating currents. *J. Gen. Physiol.* 79:21–40.
- Brum, G., and E. Ríos. 1987. Intramembrane charge movement in frog skeletal fibers. Properties of charge 2. *J. Physiol. (Camb.)*. 387: 489–517.
- Brum, G., R. Fitts, G. Pizarro, and E. Ríos. 1988. Voltage sensors of the frog skeletal muscle membrane require calcium to function in excitation–contraction coupling. *J. Physiol. (Camb.)*. 398:475–505.
- Chien, A., X. Zhao, R. Shirokov, T. Puri, C.F. Chang, D. Sun, E. Ríos, and M. Hosey. 1995. Roles of membrane-localized β subunit in the formation and targeting of functional L-type Ca^{2+} channels. *J. Biol. Chem.* 270:30036–30044.
- Conti, F., and W. Stühmer. 1989. Quantal charge redistributions accompanying the structural transitions of sodium channels. *Eur. Biophys. J.* 17:53–59.
- Felix, R., C. Gurnett, M. De Waard, and K. Campbell. 1997. Dissection of functional domains of the voltage-dependent Ca^{2+} channel $\alpha_2\delta$ subunit. *J. Neurosci.* 17:6884–6891.
- Ferreira, G., J. Yi, E. Ríos, and R. Shirokov. 1997. Ion-dependent inactivation of barium current through L-type Ca channels. *J. Gen. Physiol.* 109:449–461.
- Gurnett, C., and K. Campbell. 1996. Transmembrane auxiliary subunits of voltage-dependent ion channels. *J. Biol. Chem.* 271: 27975–27978.
- Hadley, R.W., and W.J. Lederer. 1991. Ca^{2+} and voltage inactivate Ca^{2+} channels in guinea-pig ventricular myocytes through independent mechanisms. *J. Physiol. (Camb.)*. 444:257–268.
- Hoshi, T., W.N. Zagotta, and R.W. Aldrich. 1990. Biophysical and molecular mechanisms of *Shaker* potassium channel inactivation. *Science*. 250:533–538.
- Kuo, C.-C., and B.P. Bean. 1994. Na^{+} channels must deactivate to recover from inactivation. *Neuron*. 12:819–829.
- Lauger, P. 1988. Internal motions in proteins and gating kinetics of ionic channels. *Biophys. J.* 53:877–884.
- Levitt, D. 1989. Continuum model of voltage-dependent gating. Macroscopic conductance, gating current, and single-channel behavior. *Biophys. J.* 55:489–498.
- López-Barneo, J., T. Hoshi, S.H. Heinemann, and R.W. Aldrich. 1993. Effects of external cations and mutations in the pore region on C-type inactivation of *Shaker* potassium channels. *Receptors Channels*. 1:61–71.
- Marks, T., and S.W. Jones. 1992. Calcium currents in the A7r5 smooth muscle-derived cell line. An allosteric model for Ca channel activation and dihydropyridine agonist action. *J. Gen. Physiol.* 99:367–390.
- Millhauser, G.L., E.E. Salpeter, and R.E. Oswald. 1988. Diffusion models of ion-channel gating and the origin of power law distributions from single-channel recording. *Proc. Natl. Acad. Sci. USA*. 85:1503–1507.
- Olcese, R., R. Latorre, L. Toro, F. Bezanilla, and E. Stefani. 1997. Correlation between charge movement and ionic current during slow inactivation in *Shaker* K^{+} channels. *J. Gen. Physiol.* 110:579–589.
- Press, W.H., B.P. Flannery, S.A. Teukolsky, and W.T. Vetterling. 1988–1992. Numerical recipes in C: the art of scientific computing. Cambridge University Press. 50–54.
- Shistik, E., T. Ivanina, T. Puri, M. Hosey, and N. Dascal. 1995. Ca^{2+} current enhancement by α_2/δ and β subunits in *Xenopus* oocytes: contribution of changes in channel gating and α_1 protein level. *J. Physiol. (Camb.)*. 489:55–62.
- Sigg, D., E. Stefani, and F. Bezanilla. 1994. Gating current noise produced by elementary transitions in *Shaker* potassium channels. *Science*. 264:578–582.
- Singer, D., M. Biel, I. Lotan, V. Flockerzi, F. Hofmann, and N. Dascal. 1991. The roles of the subunits in the function of the Ca channel. *Science*. 253:1553–1557.
- Shirokov, R., R. Levis, N. Shirokova, and E. Ríos. 1992. Two classes of gating current from L-type Ca channels in guinea pig ventricular myocytes. *J. Gen. Physiol.* 99:863–895.
- Shirokov, R., R. Levis, N. Shirokova, and E. Ríos. 1993. Ca^{2+} -dependent inactivation of cardiac L-type Ca channels does not affect their voltage sensor. *J. Gen. Physiol.* 102:1005–1030.
- Townsend, C., and R. Horn. 1997. Effect of alkali metal cations on slow inactivation of cardiac Na^{+} channels. *J. Gen. Physiol.* 110:23–33.
- Vassilev, P.M., T. Scheuer, and W.A. Catterall. 1988. Identification of an intracellular peptide segment involved in sodium channel inactivation. *Science*. 241:1658–1661.
- Welling, A., E. Bosse, A. Cavalié, R. Bottlender, A. Ludwig, W. Nastainczyk, V. Flockerzi, and F. Hofmann. 1993. Stable coexpression of Ca channel α_1 , β and α_2/δ subunits in a somatic cell line. *J. Physiol. (Camb.)*. 471:749–765.
- Yellen, G., D. Sodickson, T.-Y. Chen, and M.E. Yurman. 1994. An engineered cysteine in the external mouth of a K channel allows inactivation to be modulated by metal binding. *Biophys. J.* 66: 1068–1075.
- Zagotta, W.N., T. Hoshi, and R.W. Aldrich. 1990. Restoration of inactivation in mutants of *Shaker* potassium channels by peptide derived from ShB. *Science*. 250:568–571.